Quaternary Research 79 (2013) 403–412

Contents lists available at SciVerse ScienceDirect

Quaternary Research

journal homepage: www.elsevier.com/locate/yqres

Late Quaternary aeolian activity in Gonghe Basin, northeastern Qinghai-Tibetan Plateau, China

Mingrui Qiang [a,*], Fahu Chen [a], Lei Song [b], Xingxing Liu [a], Mingzhi Li [a], Qin Wang [a]

[a] MOE Key Laboratory of Western China's Environmental Systems, Research school of Arid Environment and Climate Change, Lanzhou University, Lanzhou 730000, PR China
[b] Institute of Hydrogeology and Environmental Geology, Chinese Academy of Geological Sciences, Shijiazhuang 050061, PR China

ARTICLE INFO

Article history:
Received 5 September 2012
Available online 10 April 2013

Keywords:
Aeolian activity
Aeolian sand
Paleosol
Luminescence dating
Gonghe Basin

ABSTRACT

Aeolian deposits at four sites in the Gonghe Basin were used to reconstruct the history of aeolian activity over the late Quaternary. These deposits include well-sorted aeolian sand, paleosols and/or loess. Aeolian sand represents dune-field expansion and/or dune buildup, whereas paleosols indicate stabilization of dunes, accompanying ameliorated vegetation cover. On the basis of 25 dates by optically stimulated luminescence (OSL), it appears that aeolian activities occurred episodically at 33.5, 20.3, 13.9, 11.8–11.0, 9.4, 7.8, and 5.7 (5.5) ka, which is largely consistent with the recent findings from the adjacent semi-arid areas. Aeolian sand mobility occurring during the early to mid Holocene conflicts with a climatic optimum inferred from lacustrine records in the northeastern Qinghai-Tibetan Plateau. This inconsistency may be resolved by interpreting aeolian activity as a response to decreased effective moisture due to enhanced evaporation, induced by higher summer insolation at that time, together with local terrain and its effects on moisture. Our results suggest that aeolian sand and paleosol cannot be simply ascribed to regional dry and wet climates, respectively, and they most likely reflect changes in effective moisture.

Introduction

Loess deposits on the Chinese Loess Plateau are well-known as excellent climatic records, reflecting changes in continental environments and atmospheric circulation on various time scales (e.g. An et al., 2001; Guo et al., 2002; Liu, 1985; Porter and An, 1995). To the northwest and west of the Chinese Loess Plateau, there are many large arid and semi-arid deserts (Fig. 1A) (Yang et al., 2012b; Zhu, 1980). The boundary of deserts and loess deposits is largely consistent with the northwestern margin of monsoonal regions in China (Fig. 1A).

In this marginal zone, aeolian deposits are characterized by interbedded well-sorted sand, paleosols and/or loess (Gao et al., 1993; Li et al., 2002; Lu et al., 2011; Yu and Lai, 2012). The aeolian deposits at many sites have been recently dated by optically stimulated luminescence (OSL) and interpreted as alternations of dry and wet climates induced by the Asian summer monsoon (Li et al., 2002; Liu et al., 2012; Lu et al., 2011; Mason et al., 2009; Sun et al., 2006; Xiao et al., 2002; Yang et al., 2012a; Yu and Lai, 2012). In the northeastern deserts (Hulun Buir and Otindag) of China, aeolian activity indicated by deposited dune sand occurred before 10 ka and between 3.5 and 1.7 ka; the Holocene optimum reflected by layers of paleosol was from 10 to 3.6 ka (Li et al., 2002). Similarly, three sections of aeolian deposits in central Inner Mongolia (Mu Us, Hobq and Tengger Deserts) also showed that an optimum climate prevailed from 9 to 5.6 ka and a dry climate persisted after 5.6 ka (Sun et al., 2006). However, Lu and his colleagues suggested that aeolian activity was much more intensive during the early Holocene (11.5–8 ka) than during the mid to late Holocene in these areas (Lu et al., 2005; Mason, et al., 2009). This pattern seems to be supported by the presence of aeolian sand during the early Holocene at many sites in the Qinghai Lake Basin and eastern Qaidam Basin (Liu et al., 2012; Lu et al., 2011; Yu and Lai, 2012).

The northeastern Qinghai-Tibetan Plateau is influenced by the Asian monsoon and the westerlies (Henderson et al., 2010). The area is highly sensitive to climatic changes due to its high altitude and marginal position (e.g. Zhao et al., 2010a). During the past decade, numerous reconstructions for climatic changes over the late Quaternary have been carried out on the basis of lake sediments (Herzschuh et al., 2005; Ji et al., 2005; Liu et al., 2008; Mischke et al., 2010; Shen et al., 2005; Wischnewski et al., 2011; Zhao et al., 2010a). In this area the early Holocene climate was generally warmer and wetter, but became colder and drier during the late Holocene after a mid-Holocene climatic transition. This long-term trend is similar to climatic changes recorded by speleothems from low latitudes (e.g. Dykoski et al., 2005; Fleitmann et al., 2003). In contrast, aeolian activity in the Qinghai Lake Basin occurred primarily during the early Holocene, indicating low effective moisture then (Lu et al., 2011). This finding is obviously different from the climatic trend inferred from the Qinghai lake sediments (Ji et al., 2005; Shen et al., 2005). Thus, it is suggested that aeolian deposits at various sites

* Corresponding author at: Research school of Arid Environment and Climate Change, Lanzhou University, No. 222, South Tianshui Road, Lanzhou 730000, PR China. Fax: +86 931 891 2330.
E-mail address: mrqiang@lzu.edu.cn (M. Qiang).

0033-5894/$ – see front matter
http://dx.doi.org/10.1016/j.yqres.2013.03.003

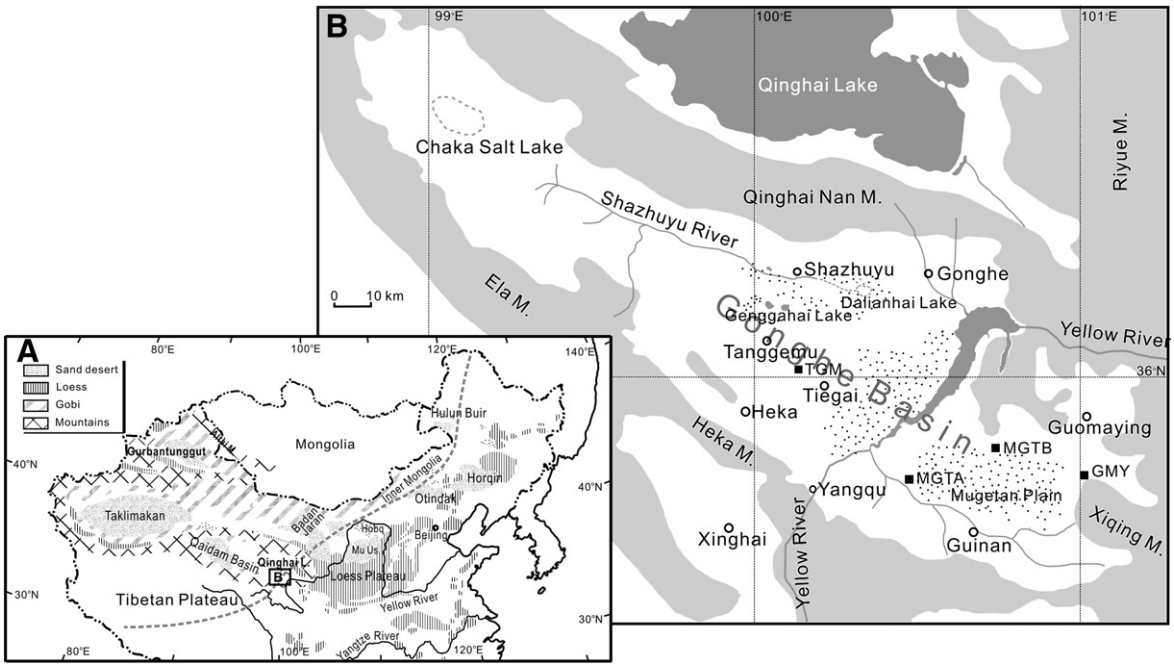

Figure 1. (A) The Gonghe Basin is located at the margin of regions dominated by the modern Asian summer monsoon, as indicated by a dashed line redrawn after Gao et al. (1962). (B) Physical environments of the Gonghe Basin. Locations of four aeolian sections are shown by solid squares.

should be investigated for further understanding of the specific responses of aeolian deposits to climatic changes.

In the Gonghe Basin, aeolian deposits are widely distributed. Dong et al. (1993) presented the uncalibrated radiocarbon ages for paleosols in the aeolian deposits at several sites. The resulting chronological framework depicted multiple wet intervals during the Holocene. Liu et al. (in press) recently used the OSL method to date an aeolian section of Lagan (LG) on the Santala Terrace. In the present article, aeolian deposits at four sites in the Gonghe Basin were dated by OSL in order to reconstruct the history of aeolian activity over the late Quaternary. The responses of aeolian deposits and lake sediments to climatic changes are discussed, providing insights into paleoclimatic reconstructions on the basis of aeolian deposits.

Study area

The Gonghe Basin (35°27′–36°56′N, 98°46′–101°22′E) has a mean altitude of 3000 m asl, with an area of 13,800 km^2. It is situated south of Qinghai Lake, separated from it by the Qinghai Nan Mountains (Fig. 1). The basin began to form as an intermountain fault basin at the end of the Eogene and subsided until the early mid-Pleistocene, as indicated by widely distributed fluvio-lacustrine sediments (Xu et al., 1984). The basin has been tectonically uplifted to a height of ~500 m relative to Yellow River since the late Pleistocene, which divided the basin into a western endorheic sub-basin and an eastern exorheic sub-basin. On the floor of the western sub-basin and on the eastern residual plains left by incision of Yellow River, the previously deposited fluvio-lacustrine sediments provide abundant fine-grained material for deflation and redeposition (Xu et al., 1982).

The mean annual precipitation in the Gonghe Basin was 310 mm (1957–2000). The mean annual temperature and mean annual potential evaporation during this period was 3.7°C and 1717 mm, respectively. More than 80% of rainfall occurs from May to September, accompanying high temperature and evapotranspiration. Strong north and northwest winds prevail in spring and winter, and the maximum wind speed in spring is 40 m s^{-1}. Aeolian activity is prevalent, resulting in extensive dune fields in the basin (Dong et al., 1993) (Fig. 1). Variations in elevation across the basin seem to affect bioclimatic zonations, which have been attributed to moisture balance (Sun et al., 2004). Desert steppe occupies the basin floor. With increases in elevation, the desert steppe gradually changes to steppe and even to meadow along the south and southeastern piedmonts.

Materials and methods

Aeolian deposits at four sites in the Gonghe Basin were selected for detailed investigation during a survey in 2010 (Figs. 1 and 2). Sample depth varied from 3.85 to 6.0 m. Section Tanggemu (TGM) is located at downwind uplands of the Tanggemu sub-basin. This section was from a gully on the left side of the road from Tiegai to Tanggemu, 7 km from Tiegai (Fig. 2A). The section mainly includes dune sand and paleosols, but also contains several interbedded alluvial layers (Fig. 3A), which we attribute to episodic sheet floods reaching the interdune area. Two sections were chosen on the Mugetan (MGT) plain in the eastern Gonghe Basin (MGTA, MGTB). These are exposed along the edges of deflation hollows, and consist of dune sand and paleosols (Figs. 2B and C). At the base of section MGTA, sheet-flow deposits were present, similar to those in section TGM. Section Guomaying (GMY) is situated in a gully on the north piedmont of Xiqing Mountain (Fig. 2D), 20 km south of Guomaying Town. The base of the section was a layer of gravel, above which aeolian sands with a thickness of 45 cm were deposited. Alluvial sand and more gravel deposits with a thickness of 30 cm overlay the aeolian sands. Above, the section consisted of interbedded loess and paleosols (Fig. 3D).

Samples for analyses of grain size and organic matter (OM) content were collected at intervals of 2, 5 or 10 cm along these sections. A total of 25 OSL dating samples was collected in light of the different subdivision boundaries of the four sections as observed in field (Figs. 2 and 3). The samples were obtained by hammering 4-cm-diameter iron tubes into the cleaned vertical sections. The tubes were covered with lids immediately after they had been taken from the section and were then sealed inside black plastic bags with tape for the samples to retain their natural water content.

Grain size and OM of the samples were analyzed at Key Laboratory of Western China's Environmental Systems (Ministry of Education), Lanzhou University. The samples were air-dried in the laboratory prior to analyses. The grain size of samples was analyzed using a

https://doi.org/10.1016/j.yqres.2013.03.003 Published online by Cambridge University Press

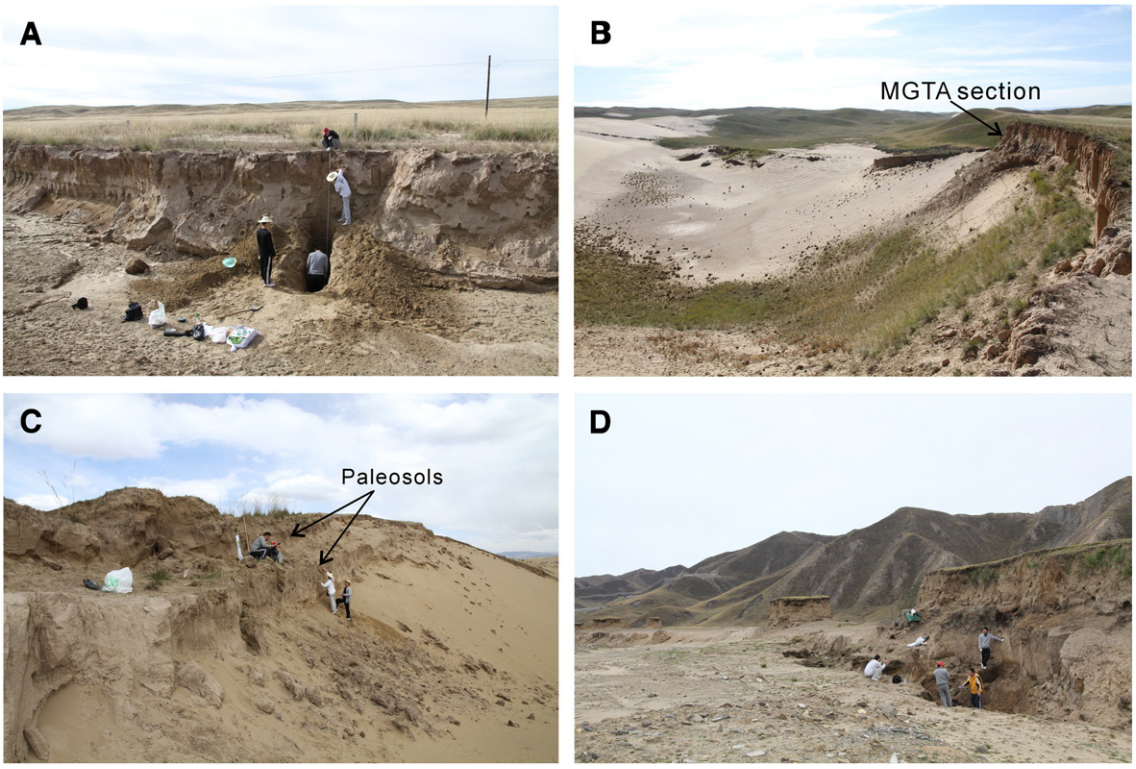

Figure 2. Photographs of landscapes of the four sections of aeolian deposition. (A) TGM, (B) MGTA, (C) MGTB, and (D) GMY.

laser particle analyzer (Malvern Instruments, Inc., Mastersizer 2000), with a measuring range of 0.02–2000 μm. Organic matter of the samples was removed by adding 10 ml of 30% H_2O_2 to 1.5 g dry sample. Carbonates were dissolved by boiling with 10 ml of 10% HCl for 10 min. Beakers were filled with 150 ml distilled water and suspended particles were left to deposit. After siphoning the supernatant water, 10 ml of 0.05 N $(NaPO_3)_6$ were added, and the residue was dispersed for 5 min in an ultrasonic bath before measurement. The OM was determined by loss on ignition (LOI) when the samples were heated at 550°C for 2 hr.

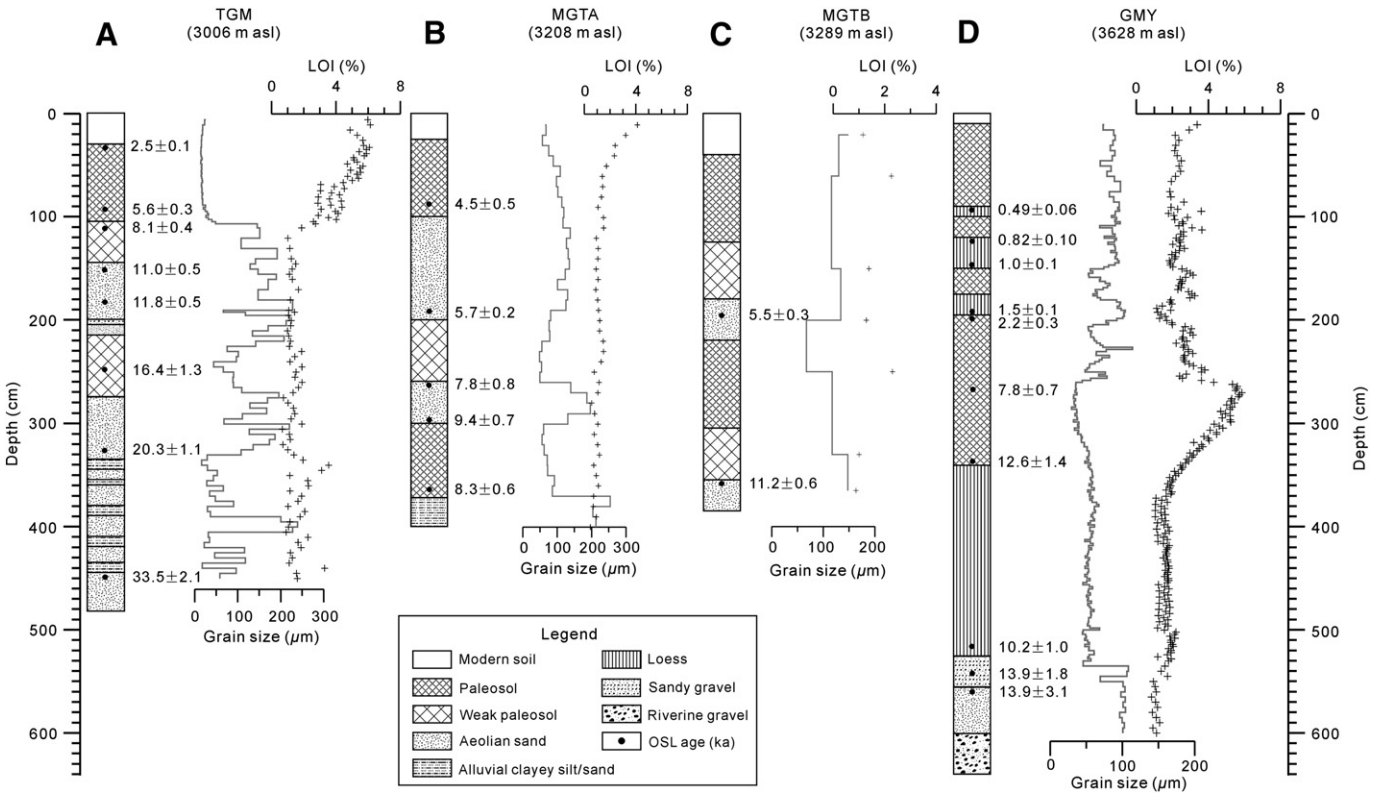

Figure 3. Lithostratigraphic units with absolute ages (ka) by OSL and proxies of mean grain size and organic matter (OM) content determined by loss on ignition (LOI).

https://doi.org/10.1016/j.yqres.2013.03.003 Published online by Cambridge University Press

Materials at the each end of the luminescence sample tube, which may have been exposed to light, were scraped away. The OSL samples from MGTA and GMY sections were reacted with 10% HCl and 20% H_2O_2 to remove carbonate and OM, respectively. The 90–125 μm fraction was then separated from the bulk by wet sieving and the quartz grains were isolated by density separation, using heavy liquid of specific gravity 2.62 and 2.75 g cm^{-3}. The quartz grains were dried and then treated with 40% HF for 40 min to remove the outer layer irradiated by alpha particles and any remaining feldspars. The grains were further treated with 1 M HCl for 10 min to remove fluorides created during the HF etching. The separated quartz grains were mounted on 10-mm-diameter aluminum discs with silicone oil as multi-grain small aliquots for measurements. The OSL samples from TGM and MGTB sections were extracted under subdued red light and separated by wet sieving with a 180-mesh sieve. The 4–11 μm fraction was separated according to Stokes' Law. Subsequently, the fine fraction was treated with 40% H_2O_2 and 30% HCl to remove OM and carbonates, and then etched with 15% H_2SiF_6 for 5 d to obtain the fine-grained quartz component. The samples were deposited on stainless steel discs, and then were dried at 40°C in an oven prior to D_e measurement.

The samples from MGTA and GMY sections were analyzed at the laboratory of Lanzhou University, using an automated Risø TL/OSL-DA-20 reader. The Risø TL/OSL-DA-20 reader was equipped with blue diodes ($\lambda = 470 \pm 20$ nm) and IR laser diodes ($\lambda = 870$ nm). The quartz OSL signal was stimulated by blue LEDs at 125°C and detected using a 7.5 mm thick U-340 filter in front of the photomultiplier tube. Equivalent dose (D_e) for each aliquot was determined using a modified single-aliquot regenerative-dose protocol (SAR) (Murray and Wintle, 2000; Wintle and Murray, 2006).

The samples from TGM and MGTB sections were analyzed at Institute of Hydrogeology and Environmental Geology, Chinese Academy of Geological Sciences, using an automated Daybreak 2200 reader. The Daybreak 2200 reader was equipped with a combined blue ($\lambda = 470 \pm 5$ nm) and infrared ($\lambda = 880 \pm 80$ nm) LED OSL unit, and a $^{90}Sr/^{90}Y$ beta source (dose rate 0.06 Gy/s). Luminescence emissions were detected by an EMI 9235QA photomultiplier tube and a 3 mm U-340 filter. The equivalent dose (D_e) for each sample was determined using a sensitivity-corrected multiple aliquot regeneration (MAR) protocol (Lu et al., 2007; Zhao et al., 2010b). The regeneration dose-response curves and OSL decay curves for 90–125 μm and 4–11 μm quartz grains are shown in Fig. 4. Dose rates were calculated from U, Th and K concentrations determined by Neutron Activation Analysis (NAA). For the 4–11 μm grains, the alpha efficiency value was taken as 0.035 ± 0.003 (Lai et al., 2008). Cosmic dose rate was calculated from present day burial depth (Prescott and Hutton, 1994).

Results

The OSL dating results were shown in Table 1 and Fig. 3. The ages were generally in chronological order, except for some inversions that are not significant relative to the dating uncertainties. Units of lithofacies of the four sections identified in field were largely consistent with changes in proxies of mean grain size and OM (Figs. 2 and 3). Aeolian sand and loess in the field showed no evidence of pedogenic alteration, and had coarse grain size and relatively low OM. Furthermore, the aeolian sand is well-sorted and distributed similarly to modern moving dune sand (Fig. 5B). We infer that the aeolian sand most likely represents episodic dune-field expansion and/or sand dune build-up. In contrast, well-developed and weakly developed paleosols are rich in pseudomycelia of secondary carbonate, are denser than aeolian sand and loess, and have much higher content of fine-grained particles (fine silts) and OM (Figs. 3 and 5A). The paleosols indicate a period of dune stabilization and probably developed when vegetation cover was able to trap silt-sized dust and prevent the dunes from deflating.

Sections TGM, MGTA and MGTB are located lower in the basin (3000–3290 m asl) than section GMY. The grain-size data (Figs. 3A–C) suggest that the sandy paleosols at these elevations originated primarily from the weathering of dune sand. For the higher GMY section (3628 m asl), loess with mean grain sizes of 50–100 μm (Fig. 3D) is the dominant sediment. This pattern suggests fine-grained dust may be entrained from the basin plain and deposited downwind. Therefore the shifts between dune sand and sandy paleosols in sections TGM, MGTA and MGTB indicate variations in the intensity of aeolian activity.

Discussion

History of aeolian activity

Strata of aeolian sand in the four sections yield a wide range of ages rather than one or more distinct clusters, although there are multiple ages from aeolian sands at 11.8–11.0 ka in sections TGM and MGTB and at around 5.5 ka in sections MGTA and MGTB (Fig. 3A–C). The lack of more distinct age clusters could be interpreted either as indicating site-specific controls on deposition and preservation (e.g. Stevens et al., 2007) and/or as a consequence of the relatively small number of OSL ages. Nonetheless, the aeolian sand units in these sections, together with the paleosols, demonstrate the occurrence of episodic aeolian activity alternating with surface stabilization by vegetation. Directly dated aeolian sand deposits occurred at 33.5, 20.3, 13.9, 11.8–11.0, 9.4, 7.8, and 5.7 (5.5) ka (Figs. 3 and 6A). The aeolian sand was mainly deposited during and shortly following the last glacial period, with no ages younger than 4.5 ka.

The greatest age (33.5 ka) of aeolian sand deposition in this study approximates the ages of aeolian deposits in sections DRE18 and GYA in Lhasa region, southern Tibetan Plateau (Lai et al., 2009). This age was obtained in the lower part of section TGM, mainly containing aeolian sand interbedded with laminated alluvial deposits. Aeolian sand deposition may have continued at this site at least until 20.3 ka, based on the limited age control. Aeolian sand deposits from the Last Glacial Maximum (LGM) have been reported from the eastern Qaidam Basin, the southeastern margin of Tengger Desert, the Horqin dunefield, and the Lhasa region (Lai et al., 2009; Qiang et al., 2010; Yang et al., 2012a; Zeng et al., 1999, 2003). At that time, the loess deposited in the central Chinese Loess Plateau was characterized by high depositional fluxes and large grain sizes (An et al., 1991), reflecting intensive dust emission and deposition.

A yellowish silty and sandy layer was identified in the entire Qinghai Lake Basin, based on the results of high-resolution (3.5 kHz) seismic-reflection (Kelts et al., 1989). According to the chronological framework of core QH2000 (Shen et al., 2005), the upper part of this layer was estimated to have been deposited at ~19 ka, indicating a period of extremely low lake level for Qinghai Lake during the LGM (Colman et al., 2007). Aeolian activity at 13.9 ka also occurred at some sites in the northeastern Qinghai-Tibetan Plateau (Liu et al., 2012; Yu and Lai, 2012) and in the Lhasa region (Lai et al., 2009). It was suggested that during the last glaciation, intense aeolian activities occurred regionally, which was attributed to the generally weakened Asian summer monsoon then (Qiang et al., in press; Shen et al., 2005; Wang et al., 2001; Yang et al., 2012a). The weakened monsoonal circulation may have reduced moisture availability and therefore vegetation cover, resulting in broad dune fields.

Early Holocene aeolian deposition occurred at 11.8–11.0 ka in sections TGM and MGTB, where the sand were similar to those at the base of section LG in the Gonghe Basin (Liu et al., in press) and at several sites in the eastern Qaidam Basin (Yu and Lai, 2012). Aeolian sands in sections MGTA and MGTB yielded ages of 9.4 ± 0.7, 7.8 ± 0.8 and 5.7 ± 0.2 (5.5 ± 0.3) ka. The closely spaced dates (8.1 ± 0.4 and 5.6 ± 0.3 ka) in section TGM suggest that there may be a sedimentary hiatus, probably due to aeolian erosion, if we consider the roughly synchronous timing between the hiatus and the aeolian activity recorded in sections MGTA and MGTB (Fig. 3).

https://doi.org/10.1016/j.yqres.2013.03.003 Published online by Cambridge University Press

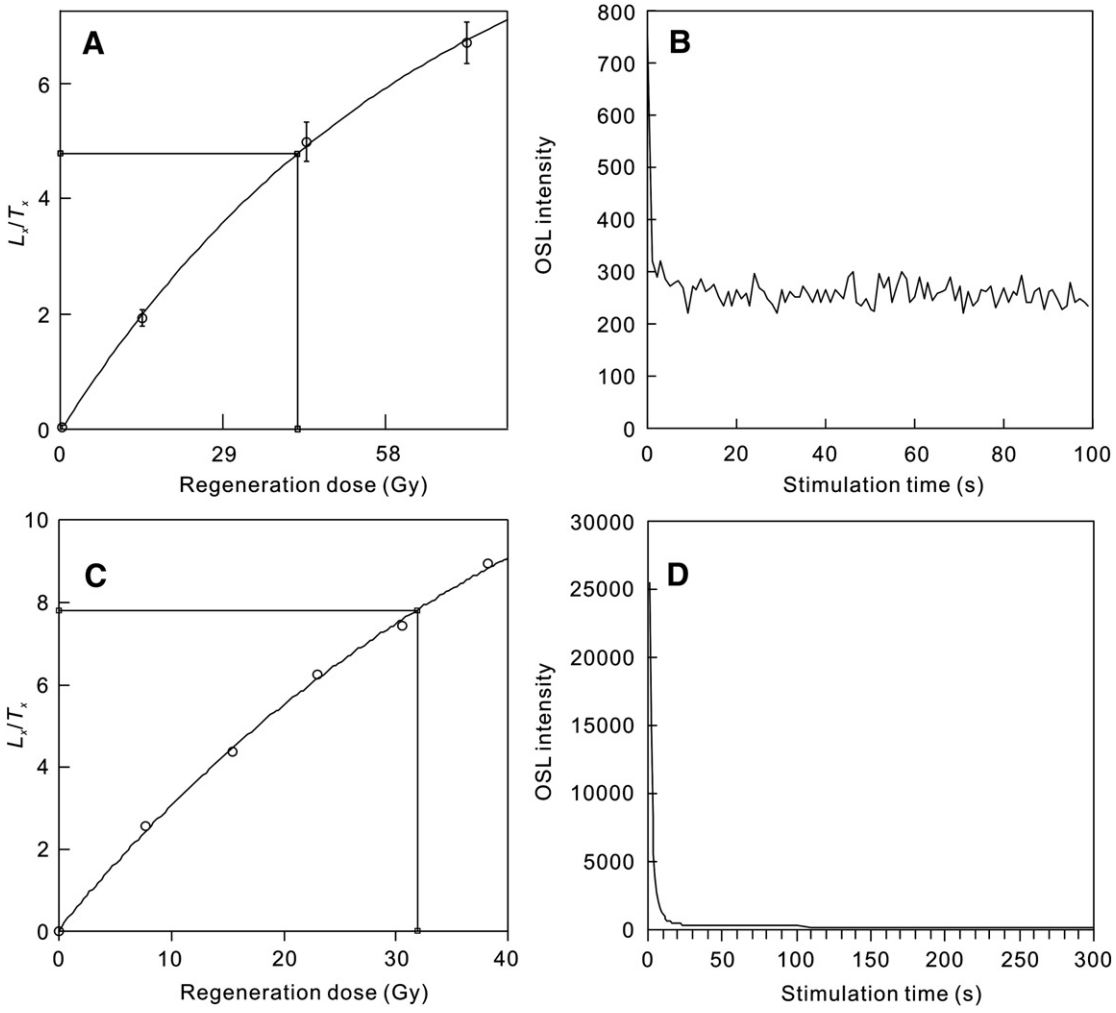

Figure 4. Corrected OSL dose-response curves and OSL signal decay curves. (A) and (B) for the coarse-grained quartz of sample MGT-A-03; (C) and (D) for the fine-grained quartz of sample TGM-03.

Table 1
OSL dating results of the studied aeolian deposits (four sections).

Sample No.	Sediment type	Depth (cm)	Water Content (%)	Grain size (μm)	K (%)	U (ppm)	Th (ppm)	Dose rate (Gy/ka)	De (Gy)	Age (ka)
TGM-01	Paleosol	32.5	17.63	4-11	1.71 ± 0.05	2.43 ± 0.10	10.8 ± 0.32	3.52 ± 0.14	8.97 ± 0.35	2.5 ± 0.1
TGM-02	Paleosol	92.5	11.79	4-11	1.94 ± 0.06	2.96 ± 0.10	12.8 ± 0.37	4.21 ± 0.17	23.56 ± 0.86	5.6 ± 0.3
TGM-03	Weak paleosol	112.5	2.86	4-11	1.68 ± 0.05	2.97 ± 0.09	10.3 ± 0.26	3.92 ± 0.16	31.92 ± 0.57	8.1 ± 0.4
TGM-04	Aeolian sand	152.5	1.86	4-11	1.71 ± 0.05	2.49 ± 0.07	9.14 ± 0.24	3.68 ± 0.15	40.39 ± 0.90	11.0 ± 0.5
TGM-05	Aeolian sand	182.5	3.72	4-11	1.43 ± 0.05	1.87 ± 0.08	9.32 ± 0.24	3.16 ± 0.13	37.20 ± 0.26	11.8 ± 0.5
TGM-06	Weak paleosol	252.5	8.89	4-11	1.54 ± 0.05	2.67 ± 0.11	10.1 ± 0.30	3.50 ± 0.14	57.60 ± 3.96	16.4 ± 1.3
TGM-07	Aeolian sand	327.5	3.70	4-11	1.43 ± 0.05	2.06 ± 0.09	10.2 ± 0.26	3.28 ± 0.13	66.77 ± 2.21	20.3 ± 1.1
TGM-08	Aeolian sand	447.5	12.25	4-11	1.63 ± 0.05	2.45 ± 0.10	9.73 ± 0.29	3.40 ± 0.14	113.77 ± 5.61	33.5 ± 2.1
MGT-B-01	Aeolian sand	197.5	2.19	4-11	1.39 ± 0.05	1.59 ± 0.07	9.21 ± 0.24	3.03 ± 0.12	16.73 ± 0.64	5.5 ± 0.3
MGT-B-02	Aeolian sand	357.5	1.44	4-11	1.45 ± 0.05	1.53 ± 0.07	9.46 ± 0.24	3.10 ± 0.12	34.86 ± 1.08	11.2 ± 0.6
MGT-A-01	Paleosol	87.5	5 ± 5	90-125	1.54 ± 0.05	1.85 ± 0.09	7.51 ± 0.24	2.92 ± 0.15	13.14 ± 1.31	4.5 ± 0.5
MGT-A-02	Aeolian sand	192.5	5 ± 5	90-125	1.57 ± 0.05	1.71 ± 0.08	8.61 ± 0.27	2.92 ± 0.16	16.78 ± 1.03	5.7 ± 0.2
MGT-A-03	Aeolian sand	262.5	5 ± 5	90-125	1.69 ± 0.05	1.7 ± 0.09	7.3 ± 0.23	2.90 ± 0.16	22.68 ± 2.03	7.8 ± 0.8
MGT-A-04	Aeolian sand	297.5	5 ± 5	90-125	1.65 ± 0.05	2.0 ± 0.09	8.57 ± 0.27	3.00 ± 0.27	28.19 ± 1.56	9.4 ± 0.7
MGT-A-05	Paleosol	362.5	5 ± 5	90-125	1.55 ± 0.05	2.05 ± 0.09	8.45 ± 0.26	2.88 ± 0.16	23.84 ± 0.98	8.3 ± 0.6
GMY-01	Loess	92.5	5 ± 5	90-125	1.5 ± 0.05	1.61 ± 0.08	8.06 ± 0.25	2.89 ± 0.15	1.43 ± 0.15	0.49 ± 0.06
GMY-02	Loess	122.5	5 ± 5	90-125	1.46 ± 0.05	1.65 ± 0.08	7.34 ± 0.23	2.79 ± 0.14	2.29 ± 0.26	0.82 ± 0.10
GMY-03	Loess	147.5	5 ± 5	90-125	1.54 ± 0.05	1.8 ± 0.08	9.35 ± 0.28	3.02 ± 0.16	3.11 ± 0.17	1.0 ± 0.1
GMY-04	Loess	192.5	5 ± 5	90-125	1.38 ± 0.05	1.6 ± 0.08	7.43 ± 0.24	2.66 ± 0.14	3.87 ± 0.27	1.5 ± 0.1
GMY-05	Paleosol	202.5	5 ± 5	90-125	1.52 ± 0.05	1.77 ± 0.08	8.53 ± 0.27	2.90 ± 0.15	6.24 ± 0.67	2.2 ± 0.3
GMY-06	Paleosol	267.5	15 ± 5	90-125	1.72 ± 0.05	2.15 ± 0.10	10.5 ± 0.32	2.98 ± 0.15	23.25 ± 1.59	7.8 ± 0.7
GMY-07	Paleosol	337.5	5 ± 5	90-125	1.48 ± 0.05	1.7 ± 0.08	8.2 ± 0.26	2.75 ± 0.15	34.62 ± 3.30	12.6 ± 1.4
GMY-08	Loess	517.5	10 ± 5	90-125	1.57 ± 0.05	2.07 ± 0.09	8.84 ± 0.27	2.74 ± 0.15	27.95 ± 2.44	10.2 ± 1.0
GMY-09	Sandy gravel	542.5	10 ± 5	90-125	1.54 ± 0.05	2.3 ± 0.10	9.23 ± 0.29	2.78 ± 0.15	38.64 ± 4.44	13.9 ± 1.8
GMY-10	Aeolian sand	557.5	5 ± 5	90-125	1.5 ± 0.05	1.51 ± 0.08	7.01 ± 0.22	2.55 ± 0.14	35.36 ± 7.65	13.9 ± 3.1

https://doi.org/10.1016/j.yqres.2013.03.003 Published online by Cambridge University Press

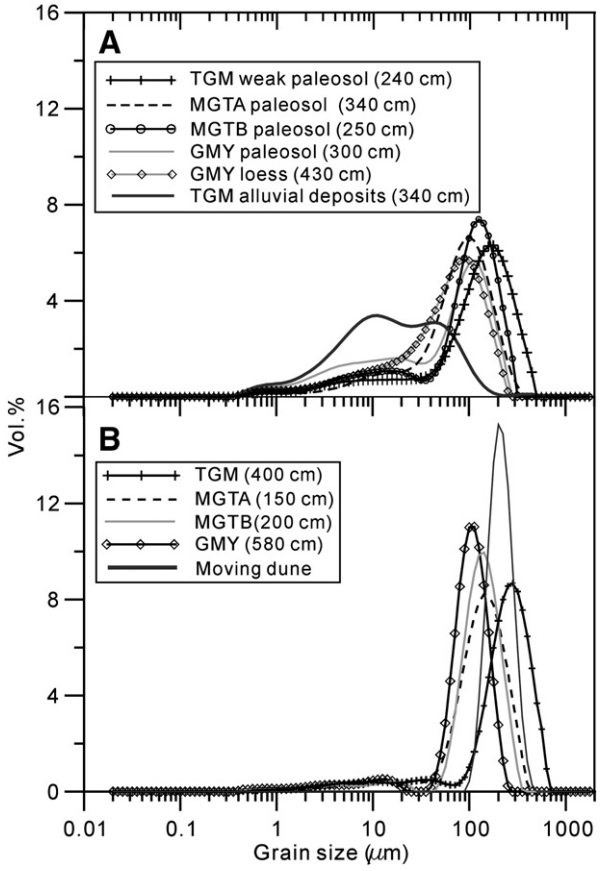

Figure 5. Grain size frequency distributions for samples of paleosols, loess and alluvial deposits from sections TGM, MGTA, MGTB and GMY (A) and for samples of aeolian sand from the four sections and modern moving dune (B). Depths of the samples are given in brackets.

In order to further understand the occurrences of aeolian activity in the Gonghe Basin over the late Quaternary, we collected the previously published OSL ages of aeolian samples from the northeastern Qinghai-Tibetan Plateau (Lu et al., 2011; Liu et al., 2012; Yu and Lai, 2012; Liu et al., in press; see Supplement Table A1 for details). These samples were divided into three groups, i.e. aeolian sand, loess, and paleosol, according to lithofacies as described by the authors. Combined with the OSL ages in this study, 111 ages in total from 25 sites were plotted to extract paleoenvironmental information using a probability density function (PDF) (e.g. Lai et al., 2009; Singhvi et al., 2001; Telfer and Thomas, 2007; Yu and Lai, 2012). It is noteworthy that an OSL-age cluster produced by PDF plots might reflect a higher and accidental sampling density along aeolian sections and/or an enhanced accumulation of aeolian deposits (Singhvi et al., 2001). It was suggested, however, that sampling in a systematic manner with a great sampling density would minimize this effect (Telfer and Thomas, 2007). Thus, the large number of OSL ages compiled here most likely represents random, overall occurrences of aeolian deposition in this region. The clusters seen in PDF plots could be interpreted as indicating enhanced aeolian deposition, and the accidental sampling density may have a minor effect on the age distributions.

Fig. 6B shows the distributions of ages of preserved aeolian deposits. Four age clusters of aeolian sand were detected centering at 11.6, 9.4, 5.6 and 0.6 ka, and aeolian sand may not have accumulated from 5 to 1 ka and since 0.4 ka. This distribution appears to be in anti-phased with to paleosol ages in this region; paleosols developed episodically after 5.5 ka, despite an age cluster appearing between 10 and 8 ka. Several episodically enhanced loess accumulations were observed after 6 ka. The age cluster of loess between 14 and 9 ka was largely consistent with the most remarkable age cluster of aeolian sand, probably reflecting intensive dust emission from source areas due to aeolian activity if it is assumed that loess deposits always deposit downwind. Although OSL ages of aeolian sand from the Gonghe Basin are sparse and the number is relatively small, the ages largely correspond to the clusters of aeolian sand identified by the PDF plots with additional independent OSL ages (Figs. 6A and B). This suggests that aeolian activity during the early to mid Holocene in the Gonghe Basin were intensive and/or frequent on a large spatial scale, and that the paleosols occurred primarily during the late Holocene in this region. Early Holocene aeolian activity was also found at 10.5–7 ka in the Donggi Cona catchment, ~160 km southwest of the Gonghe Basin (Stauch et al., 2012), at 8–7 ka in the Lhasa region (Lai et al., 2009), and at 10–8 ka in northern China (Lu et al., 2005; Mason et al., 2009).

Comparison with paleoclimatic records

At the present, there are three major dune fields in the Gonghe Basin (Fig. 1B), which mainly consist of fully active barchan and barchannoid ridge dunes, nearly devoid of vegetation (Dong et al., 1993). The presence of dune fields would be a response to windiness, sand supply, and favorable deposition places. However, human activity may have played a significant role in expansion of these dune fields due to disturbance of ground surface by overly collecting firewood, grazing, and reclaiming farmlands, especially after the founding of the People's Republic of China in 1949 (Dong et al., 1993). The archaeological findings suggested that in the Qinghai Lake Basin, human occupation began at 9 ka (Rhode et al., 2007) and even as early as 14.3 ka (Sun et al., 2012), but artifact contents from excavated sites suggested that the sites may have serviced as base camps for hunting until 5 ka (Rhode et al., 2007). Based on a suit of palynological and geomorphological data, Schlütz and Lehmkuhl (2009) found that first signs of nomadic presence appeared as early as 7.2 ka and the Poaceae-rich natural vegetation was transformed by nomadic grazing to *Kobresia*-pastures at 5.9–2.7 ka in the Nianbaoyeze Mountains at the eastern margin of Tibetan Plateau. Fossil pollen records available from monsoonal China suggest that human disturbance may have became an increasingly important factor for changes in vegetation over the last 2 ka (Zhao et al., 2009). Human activity probably played an important role in aeolian activity at around 0.8 and 0.2 ka in the Horqin dunefield (Yang et al., 2012a). Thus, human activity might have affected vegetation, and hence dune evolution at some local sites early in the Holocene, but there are no evidence showing consistent occurrence of dune sand on a large scale induced by human activity during most part of the Holocene. With this respect, the history of aeolian activity in the Gonghe Basin presented above would reflect climate-related conditions over the late Quaternary.

Climatic changes during the Holocene across China have been discussed by many researchers. An et al. (2000) investigated the spatial and temporal distributions of effective moisture across the monsoonal areas of China during the Holocene, based on lake levels, pollen profiles and loess/paleosol records. They proposed that the Holocene monsoon optimum, as defined by the peak East Asian summer monsoon precipitation, exhibits a clear diachronism with a southeast retreat trend. The effective maximum appeared at around 9 ka in the north and northwest and progressively later toward the south and southeast; the optimum belt retreated to the middle and lower reaches of the Yangtze River during the mid Holocene. However, this finding differs from the results reviewed by Feng et al. (2006). The Holocene climatic optimum occurred nearly contemporaneously between 8 and 5 ka in Xinjiang, on the Inner Mongolian Plateau, and on the northwestern Chinese Loess Plateau, whereas the northern Tibetan Plateau experienced a climatic optimum at 10–8 ka (Feng et al., 2006). Similarly, He et al. (2004) also found the Holocene optimum (10–7.2 ka) began and terminated earlier in high-altitude regions of

https://doi.org/10.1016/j.yqres.2013.03.003 Published online by Cambridge University Press

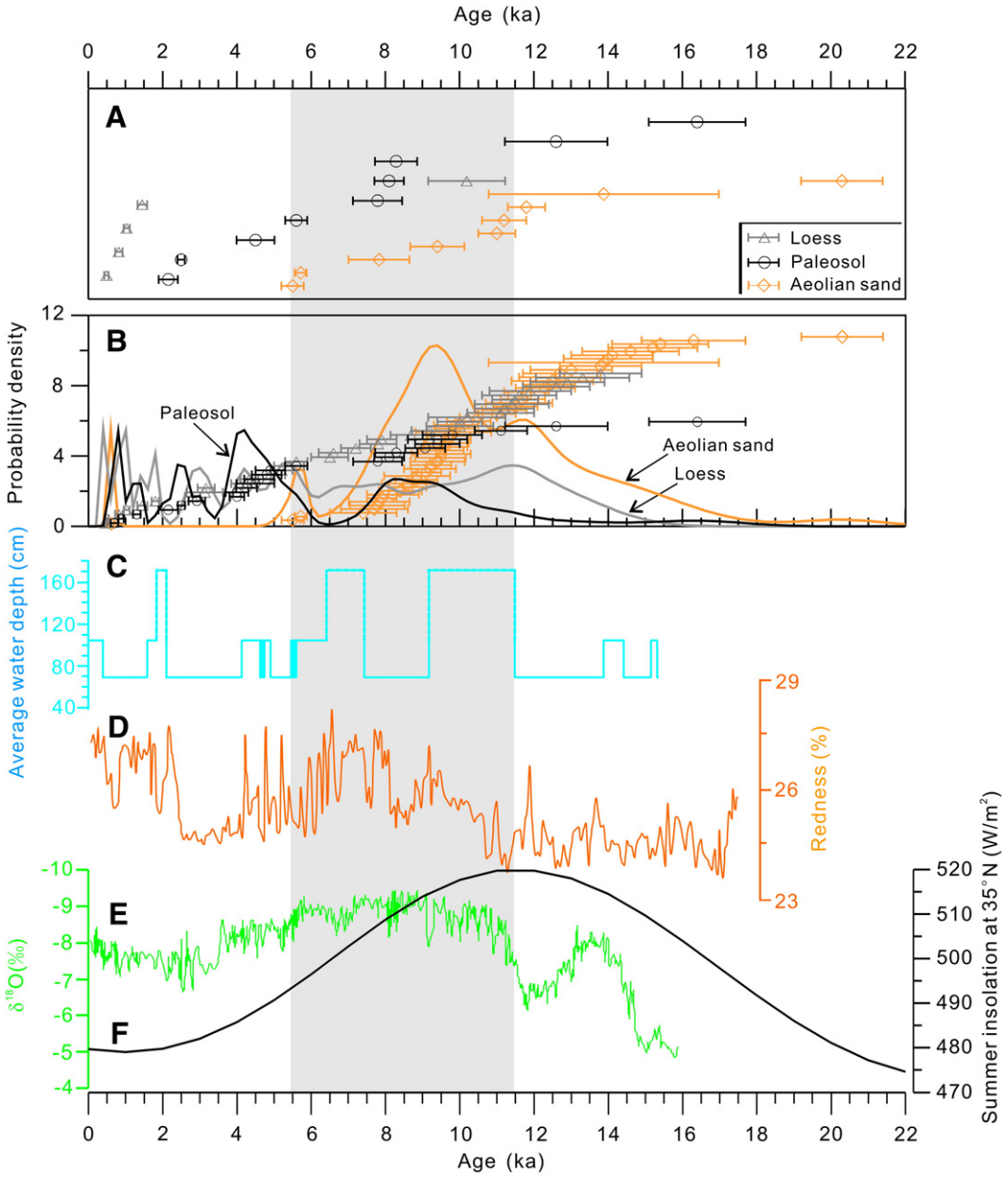

Figure 6. Comparisons of aeolian activity history and other paleoclimatic records. (A) OSL ages from aeolian sand, loess, and paleosols of the four sections in the Gonghe Basin. (B) Probability density plot for the OSL ages of aeolian samples from the northeastern Qinghai-Tibetan Plateau (data after Lu et al., 2011; Liu et al., 2012; Yu and Lai, 2012; Liu et al., in press). The legends are the same as (A). (C) Lake-level fluctuations reconstructed using the macrofossil assemblages from Genggahai Lake in the Gonghe Basin (Qiang et al., in press). (D) Redness variations of core QH2000 from Qinghai Lake (Ji et al., 2005), indicating changes in precipitation. (E) $\delta^{18}O$ of the D4 stalagmite calcite from Dongge Cave (Dykoski et al., 2005). (F) Monthly average insolation (June) (Berger and Loutre, 1991). Gray bar highlights the period of the early to mid Holocene.

western China than at lower elevations in eastern China. In the arid and semi-arid areas of China, however, significant increases in effective moisture occurred after 8 ka, probably caused by either enhanced water-vapor transport by the westerlies to these areas when the North Atlantic sea-surface temperature increased (Chen et al., 2008; Jin et al., 2012), and/or reduced subsidence of dry air masses relative to the early Holocene in the areas to the north and northeast of the Tibetan Plateau (Herzschuh, 2006; Mason et al., 2009). In regions dominated by the Asian monsoon, synthesis results of 31 pollen records indicate that a humid climate generally characterized the early to mid Holocene, and a drier climate prevailed during the late Holocene (Zhao et al., 2009). This pattern is similar to that of oxygen-isotope synthesis results of lake sediments (Zhang et al., 2011), suggesting that the Holocene climate was broadly synchronous across the monsoonal region.

Despite the spatial difference of the Holocene climatic optimum across China, there is growing evidence showing a strong Asian summer monsoon on the northeastern Qinghai-Tibetan Plateau during the early to mid Holocene (e.g. Zhao and Yu, 2012). Fossil pollen and geochemical variables of the sequential sediments (core QH2000) from Qinghai Lake suggested that the optimum climate started at the beginning of the Holocene in a gradual manner and persisted until 4.5 ka, and the climate gradually became colder and drier afterwards (Shen et al., 2005). Ji et al. (2005) used redness (iron-oxide content) of the sediments from Qinghai Lake, reflecting erosion from nearby red beds by fluvial means, and reconstructed changes in precipitation intensity (Fig. 6D).

https://doi.org/10.1016/j.yqres.2013.03.003 Published online by Cambridge University Press

The independent data strongly support the Holocene climatic pattern proposed formerly (Lister et al., 1991; Shen et al., 2005). Similarly, total organic carbon, total nitrogen and mineral assemblages of core sediments from Chaka Salt Lake (Fig. 1B for location) illustrated a warm and humid climate between 11.4 and 5.3 ka and a clod and dry period after 5.3 ka (Liu et al., 2008). Based on the refined date framework, Zhao et al. (2010a) suggested that a high lake level of Hurleg Lake occurred from 10 to 8 ka in the eastern Qaidam Basin, as a result of enhanced river inflows induced by the strengthening Asian monsoon. At the northeastern margin of the Qaidam Basin, water level of Xiao Qaidam Lake may have been up to ~10 m higher than today from 11 to 3 ka (Sun et al., 2010).

Genggahai Lake is located at the central Gonghe Basin (Fig. 1B). This lake is a small (~2 km^2), shallow lake, occupied by dense submerged vegetation. Spatial distributions of the aquatic macrophytes are highly associated with water depth. Macrofossil assemblages from core sediments showed that, in the past, dominant taxa were almost the same as those of today (Qiang et al., in press). This lake is fed mainly by ground water. Meltwater is not a significant contribution to the lake, because most precipitation occurs in summer and the altitudes (<4,000 m asl) of the surrounding mountains are not high enough to develop massive glaciers. Furthermore, the lake has a small ratio of lake area to its drainage area, and thus water-level fluctuations of this lake most likely reflect changes in precipitation (e.g. Morrill, 2004). Lake level was low during the late glacial period. From 11.4 to 6.3 ka, a remarkably high water level was punctuated by a period of relatively low water level between 9.2 and 7.4 ka. During the late Holocene, lake level was characterized by long-term low levels with frequent fluctuations (Fig. 6C; Qiang et al., in press). Regardless of changes on centennial to millennial time scales, the general lake-level fluctuations of Genggahai Lake largely coincide with the climatic records from adjacent areas (Herzschuh et al., 2005, 2009; Ji et al., 2005; Kramer et al., 2010; Lister et al., 1991; Liu et al., 2008; Mischke et al., 2010; Morrill et al., 2006; Shen et al., 2005; Wang et al., 2010; Wischnewski et al., 2011). The high lake levels also are in line with strengthened circulation of the Asian summer monsoon during the early to mid Holocene, as recorded by speleothems and marine sediments from low latitudes (cf. Figs. 6C and E) (Dykoski et al., 2005; Fleitmann et al., 2003; Gupta et al., 2003; Wang et al., 2005). The large-scale climate similarities could be attributed to the overall increase in temperature across the Eurasian continent (e.g. Stuiver et al., 1995). Enhanced thermal contrast between land and sea in spring and summer can fuel intense circulation of the Asian monsoon (Morrill et al., 2003; Overpeck et al., 1996). Precipitation belt driven by the monsoon may have shifted northwards and brought about much more rainfall on the northeast Qinghai-Tibetan Plateau at that time. This was evidenced by the high levels of lakes in this region (Lister et al., 1991; Qiang et al., in press; Sun et al., 2010; Zhao et al., 2010a) and by the magnetism-based reconstruction of precipitation at Duowa (Maher and Hu, 2006).

It is impossible to compare the aeolian activity presented above with the climatic oscillations on a small time scale, because of the low resolution of dune sand sequences and the discrete OSL ages. Nonetheless, given that the climatic optimum on multi-millennial timescales in the northeastern Qinghai-Tibetan Plateau is acceptable, the occurrences of aeolian sand activity during the early to mid Holocene seem to obviously contradict the favored view that aeolian sand depositions are always indicative of arid phases (e.g. Partridge, 1993; Telfer and Thomas, 2007).

Paleoclimatic implications

The contradiction between the Holocene aeolian activity and the climatic optimum raises questions as to which climatological factors are the major controls on aeolian activity, and whether some of those factors can allow aeolian activity at times of relatively high precipitation as inferred from the early to mid Holocene lake sediments.

Aeolian activity and sand mobility can be regarded as a function of vegetation cover, wind strength, and supply of sand-sized particles (Lancaster, 1995). In the Gonghe Basin, ancient fluvio-lacustrine sediments are ubiquitous, and the sand supply therefore is not a restricting factor for aeolian activity. There is little evidence for changes in wind strength over the Holocene. Recently, Wang et al. (2012) pointed out that the East Asian winter monsoon displayed the maximums at 10–8.5 ka and 7–5 ka, based on the diatom data from Huguang Maar Lake in southern China. However, dust fluxes and elemental compositions of a Hongyuan peat sequence from the eastern Tibetan Plateau suggested that the winter monsoon was generally weak from the early to mid Holocene, and then enhanced during the late Holocene (Yu et al., 2011). In this study, the aeolian dune sand not only occurred during the early to mid Holocene, but also during the last glaciation. It is well-known that wind strength was stronger during glacial than during interglacial times (An et al., 1991; Liu and Ding, 1998). Thus, wind strength can not fully explain the occurrences of aeolian activity. Additionally, grain size of lower part of section GMY was overall finer than that of the deposits after ~7.8 ka (Fig. 3D). Assuming that the loess deposits of section GMY were mainly derived from dune fields in this basin, finer dust particles during the early Holocene may indicate weak wind conditions if widely active dune fields are considered as dust source areas at that time and distance between the source areas and the depositional site was shortened; whereas coarser particles of the upper deposits in this section perhaps represent enhanced wind regimes, since dune fields may have been broadly fixed in the late Holocene. In fact, at the present, dune fields are distributed as patches, where there is little or no vegetation, surrounded by areas where vegetation stabilizes surficial materials. The observation suggests that (1) wind strength may have a minor effect on dune formation, since strong winds are always ubiquitous across the whole basin in spring and winter (Dong et al., 1993), and (2) factors influencing vegetation cover are important. On the basis of investigations on dune mobility in recent decades in semi-arid northern China, Mason et al. (2008, 2009) proposed that effective moisture, the balance between precipitation and potential evapotranspiration, plays an important role in sand mobility through its influence on vegetation cover. The few fossil pollen data sets from the Gonghe Basin clearly demonstrates that pollen abundance was lower in aeolian sand deposits than in paleosols (Dong et al., 1993), which is consistent with the changes in OM measured in the present study (Fig. 3). Therefore, we argue that in the study area effective moisture affects aeolian sand mobility by controlling changes in vegetation cover.

The long-term trend in climatic changes as recorded by the lake sediments largely follows the variations in summer solar insolation in the North Hemisphere (Figs. 6C, D and F). During the early Holocene, the intense insolation may cause increased monsoonal precipitation in the northeastern Qinghai-Tibetan Plateau, but from the viewpoint of vegetation and soil moisture, the effect may have been offset by high evaporation due to high temperature, induced by the increased insolation (Berger and Loutre, 1991; Lu et al., 2011; Mason et al., 2009). Temperatures were up to 2°C warmer than today in the eastern Tibetan Plateau at that time (Schlütz and Lehmkuhl, 2009). The resulting low level of effective moisture then may have led to the inferred dune mobility in the study area. The moisture balance tended to ameliorate during the late Holocene, as indicated by paleosol formation at many sites in the northeastern Qinghai-Tibetan Plateau (Liu et al., 2012; Lu et al., 2011; Yu and Lai, 2012).

Understanding the mobilization and deposition of sand under the optimum climate of the early to mid Holocene in the study area requires us to consider the local terrain and its effects. Aeolian deposits are accumulated in areas higher in the landscape than the basins that contain lakes. Elevation difference could result in water redistribution within the basin. Enhanced precipitation in the study area can effectively increase soil moisture, but water in excess of storage or evaporation/evapotranspiration must flow toward the lakes. This may explain the inconsistency between the observed high stand of Genggahai Lake and the coeval occurrence of aeolian sand in the basin during the early to

https://doi.org/10.1016/j.yqres.2013.03.003 Published online by Cambridge University Press

mid Holocene, assuming that increased soil moisture was offset locally by higher evaporation. Evidence, probably supporting this inference, is that in the Donggi Cona catchment, aeolian sand and colluvial sediments by fluvial processes occurred nearly synchronously from the early to mid Holocene (Stauch et al., 2012). On the other hand, effective moisture is characterized by spatial variations across the Gonghe Basin, due to an integrative effect of temperature, precipitation and elevation (Sun et al., 2004). Illustrating this is the well-developed paleosol that appeared at ~7.8 ka in section GMY, suggesting that a favorable level of effective moisture for pedogenic weathering was reached at this site, while aeolian sand occurred nearly synchronously in the MGTA section (Figs. 3B and D). These surface processes seem to disentangle the causal linkage between monsoon strength and aeolian activity, but to which extent these processes affect aeolian activity remains to be assessed.

In summary, aeolian sand mobility and high lake level in the Gonghe Basin seem to vary in phase with higher summer insolation during the early to mid Holocene. However, the occurrence of aeolian sand probably represents a low level of effective moisture, as an integrative result of higher temperature, redistribution of meteoric water and variations in elevation, rather than regional aridity. As for the late Holocene, enhanced effective moisture does not necessarily require an increase in regional precipitation, but may result from moisture balance between lower precipitation and lower evaporation due to decreased temperature. It is noteworthy, therefore, that paleoclimatic changes inferred from aeolian deposits have to be interpreted cautiously as wet or dry climates.

Conclusions

Direct OSL dating on fossil aeolian sand from the Gonghe Basin shows that over the late Quaternary the strongest aeolian activity occurred at 33.5, 20.3, 13.9, 11.8–11.0, 9.4, 7.8, and 5.7 (5.5) ka. Aeolian activity not only appeared episodically during the last glaciation, but following the deglaciation during the early to mid Holocene. Aeolian sand mobility then seems not to be explained by increased aridity, since lacustrine records clearly demonstrate enhanced summer precipitation, due to the Asian monsoon, at that time. Effective moisture can affect vegetation cover, and may explain the observed dune mobility. Early to mid Holocene sand mobility could have resulted from high evaporation due to high temperature, assuming that increased soil moisture was offset locally by higher evaporation. However, water in excess of storage or evaporation/evapotranspiration must flow toward the lakes and then give rise in higher water levels in lakes. Late Holocene paleosols indicate a high level of effective moisture then, but must not require increased precipitation, according to the adjacent lake records.

Our results suggest that aeolian deposition in the Gonghe Basin is variable from site to site. Thus, reconstructing climatic and environmental changes there requires studying aeolian and other deposits from many sites distributed across the basin. Furthermore, interpretation of aeolian deposits needs to be combined with time series of climatic changes from other geological archives in context of regional climate variability.

Supplementary data to this article can be found online at http://dx.doi.org/10.1016/j.yqres.2013.03.003.

Acknowledgments

We thank H. Zhao, C.M. Wang, Y.X. Fan and T.L. Fan for their assistance in OSL dating and data analyses. We thank Prof. J.A. Mason and an anonymous reviewer for their constructive comments to greatly improve the early version of this paper. The research was supported by the National Science Foundation of China (grants 41271219, 40830105), the National Basic Research Program of China (grants 2010CB403301 and 2012CB956102), and the MOE Program for New Century Excellent Talents in University to M. Qiang.

References

An, Z.S., Kukla, G.J., Porter, S.C., Xiao, J.L., 1991. Late Quaternary dust flow on the Chinese loess plateau. Catena 18, 125–132.
An, Z.S., Porter, S.C., Kutzbach, J.E., Wu, X.H., Wang, S.M., Liu, X.D., Li, X.Q., Zhou, W.J., 2000. Asynchronous Holocene optimum of the East Asian monsoon. Quaternary Science Reviews 19, 743–762.
An, Z.S., Kutzbach, J.E., Prell, W.L., Porter, S.C., 2001. Evolution of Asian monsoons and phased uplift of the Himalaya-Tibetan plateau since Late Miocene times. Nature 411, 62–66.
Berger, A., Loutre, M.F., 1991. Isolation values for the climate of the last 10 million years. Quaternary Science Reviews 10, 297–317.
Chen, F.H., Yu, Z.C., Yang, M.L., Ito, E., Wang, S.M., Madsen, D.B., Huang, X.Z., Zhao, Y., Sato, T., Birks, H.J.B., Boomer, I., Chen, J.H., An, C.B., Wünnermann, B., 2008. Holocene moisture evolution in arid central Asia and its out-of-phase relationship with monsoon history. Quaternary Science Reviews 27, 351–364.
Colman, S.M., Yu, S.-Y., An, Z.S., Shen, J., Henderson, A.G.G., 2007. Late Cenozoic climate changes in China's western interior: a review of research on Lake Qinghai and comparison with other records. Quaternary Science Reviews 26, 2281–2300.
Dong, G.R., Gao, S.Y., Jin, J., 1993. Desertification and Controls in the Gonghe Basin, Qinghai Province. Science Press, Beijing, pp. 1–166 (in Chinese with English abstract).
Dykoski, C.A., Edwards, R.L., Cheng, H., Yuan, D.X., Cai, Y.J., Zhang, M.L., Lin, Y.S., Qing, J.M., An, Z.S., Revenaugh, J., 2005. A high-resolution, absolute-dated Holocene and deglacial Asian monsoon record form Dongge Cave, China. Earth and Planetary Science Letters 233, 71–86.
Feng, Z.-D., An, C.B., Wang, H.B., 2006. Holocene climatic and environmental changes in the arid and semi-arid areas of China: a review. The Holocene 16, 119–130.
Fleitmann, D., Burns, S.J., Mudelsee, M., Neff, U., Kramers, J., Mangini, A., Matter, A., 2003. Holocene forcing of Indian monsoon recorded in a stalagmite from southern Oman. Science 300, 1737–1739.
Gao, Y.X., Xu, S.Y., Guo, Q.Y., Zhang, M.L., 1962. Monsoon regions in China and regional climates. In: Gao, Y.X. (Ed.), Some Problems on East-Asia monsoon. Science Press, Beijing, pp. 49–63 (in Chinese).
Gao, S.Y., Chen, W.N., Jin, H.l, Dong, G.R., Li, B.S., Yang, G.S., Lin, L.Y., Guan, Y.Z., Sun, Z., Jin, J., Zhang, Y.T., Cao, J.S., 1993. Preliminary study on the Holocene evolution of the NW desert margin in the monsoon region of China. Science in China Series B 23, 202–208 (in Chinese).
Guo, Z.T., Ruddiman, W.F., Hao, Q.Z., Wu, H.B., Qiao, Y.S., Zhu, R.X., Peng, S.Z., Wei, J.J., Yuan, B.Y., Liu, T.S., 2002. Onset of Asian desertification by 22 Myr ago inferred from loess deposits in China. Nature 416, 159–162.
Gupta, A.K., Anderson, D.M., Overpeck, J.T., 2003. Abrupt changes in the Asian southwest monsoon during the Holocene and their links to the North Atlantic Ocean. Nature 421, 354–357.
He, Y., Theakstone, W.H., Zhang, Z.L., Zhang, D., Yao, T.D., Chen, T., Shen, Y.P., Pang, H.X., 2004. Asynchronous Holocene climatic change across China. Quaternary Research 61, 52–63.
Henderson, A.C.G., Holmes, J.A., Leng, M.J., 2010. Late Holocene isotope hydrology of Lake Qinghai, NE Tibetan Plateau: effective moisture variability and atmospheric circulation changes. Quaternary Science Reviews 29, 2215–2223.
Herzschuh, U., 2006. Palaeo-moisture evolution in monsoonal Central Asia during the last 50,000 years. Quaternary Science Reviews 25, 163–178.
Herzschuh, U., Zhang, C.J., Mischke, S., Herzschuh, R., Mohammadi, F., Mingram, B., Kqrschner, H., Riedel, F., 2005. A late Quaternary lake record from the Qilian Mountains (NW China): evolution of the primary production and the water depth reconstructed from macrofossil, pollen, biomarker, and isotope data. Global and Planetary Change 46, 361–379.
Herzschuh, U., Kramer, A., Mischke, S., Zhang, C.J., 2009. Quantitative climate and vegetation trends since the late glacial on the northeastern Tibetan Plateau deduced from Kuocha Lake pollen spectra. Quaternary Research 71, 162–171.
Ji, J.F., Shen, J., Balsam, W., Chen, J., Liu, L.W., Liu, X.Q., 2005. Asian monsoon oscillations in the northeastern Qinghai–Tibet Plateau since the late glacial as interpreted from visible reflectance of Qinghai Lake sediments. Earth and Planetary Science Letters 233, 61–70.
Jin, L.Y., Chen, F.H., Morrill, C., Otto-Bliesner, B.L., Rosenbloom, N., 2012. Causes of early Holocene desertification in arid central Asia. Climate Dynamics 38, 1577–1591.
Kelts, K.R., Chen, K.Z., Lister, G.S., Yu, J.Q., Gao, Z.H., Niessen, N., Bonani, G., 1989. Geological fingerprints of climate history: a cooperative study of Qinghai Lake, China. Eclogae Geologicae Helvetiae 82, 167–182.
Kramer, A., Herzschuh, U., Mischke, S., Zhang, C.J., 2010. Holocene treeline shifts and monsoon variability in the Hengduan Mountains (southeastern Tibetan Plateau), implications form palynological investigations. Palaeogeography, Palaeoclimatology, Palaeoecology 286, 23–41.
Lai, Z.P., Zöller, L., Fuchs, M., Brückner, H., 2008. Alpha efficiency determination for OSL of quartz extracted from Chinese loess. Radiation Measurements 43, 767–770.
Lai, Z.P., Kaiser, K., Brückner, H., 2009. Luminescence-dated aeolian deposits of late Quaternary age in the southern Tibetan Plateau and their implications for landscape history. Quaternary Research 72, 421–430.
Lancaster, N., 1995. Geomorphology of Desert Dunes. Routledge, London and New York, pp. 228–254.
Li, S.-H., Sun, J.M., Zhao, H., 2002. Optical dating of dune sands in the northeastern deserts of China. Palaeogeography, Palaeoclimatology, Palaeoecology 181, 419–429.

Lister, G.S., Kelts, K., Chen, K.Z., Yu, Z.Q., Niessen, F., 1991. Lake Qinghai, China: closed-basin lake levels and the oxygen isotope record for ostracoda since the latest Pleistocene. Palaeogeography, Palaeoclimatology, Palaeoecology 84, 141–162.
Liu, T.S., 1985. Loess and Environment. China Ocean Press, Beijing.
Liu, T.S., Ding, Z.L., 1998. Chinese loess and the paleomonsoon. Annual Review of Global Earth and Planetary Sciences 26, 111–145.
Liu, X.Q., Dong, H.L., Rech, J.A., Matsumoto, R., Yang, B., Wang, Y.B., 2008. Evolution of Chaka Salt Lake in NW China in response to climatic change during the Latest Pleistocene–Holocene. Quaternary Science Reviews 27, 867–879.
Liu, X.J., Lai, Z.P., Yu, L.P., Sun, Y.J., Madsen, D., 2012. Luminescence chronology of aeolian deposits from the Qinghai Lake area in the Northeastern Qinghai-Tibetan Plateau and its palaeoenvironmental implications. Quaternary Geochronology 10, 37–43.
Liu, B., Jin, H.L., Sun, L.Y., Sun, Z., Su, Z.Z., Zhang, C.X., in press. Holocene climatic change revealed by aeolain deposits from the Gonghe Basin, northeastern Qinghai-Tibetan Plaeau. Quaternary International, doi: 10.1016/j.quaint.2012.05.003.
Lu, H.Y., Miao, X.D., Zhou, Y.L., Mason, J., Swinehart, J., Zhang, J.F., Zhou, L.P., Yi, S.W., 2005. Late Quaternary aeolian activity in the Mu Us and Otindag dune fields (north China) and lagged response to insolation forcing. Geophysical Research Letters 32, L21716. http://dx.doi.org/10.1029/2005GL024560.
Lu, Y.C., Wang, X.L., Wintle, A.G., 2007. A new OSL chronology for dust accumulation in the last 130,000 yr for the Chinese Loess Plateau. Quaternary Research 67, 152–160.
Lu, H.Y., Zhao, C.F., Mason, J., Yi, S.W., Zhao, H., Zhou, Y.L., Ji, J.F., Swinehart, J., Wang, C.M., 2011. Holocene climatic changes revealed by aeolian deposits from the Qinghai Lake area (northeastern Qinghai-Tibetan Plateau) and possible forcing mechanisms. The Holocene 21, 297–304.
Maher, B.A., Hu, M.Y., 2006. A high-resolution record of Holocene rainfall variations from the western Chinese Loess Plateau: antiphase behaviour of the African/Indian and East Asian summer monsoons. The Holocene 16, 309–319.
Mason, J.A., Swinehart, J.B., Lu, H.Y., Miao, X.D., Cha, P., Zhou, Y.L., 2008. Limited change in dune mobility in response to a large decrease in wind power in semi-arid north China since 1970s. Geomophology 102, 351–363.
Mason, J.A., Lu, H., Zhou, Y., Miao, X., Swinehart, J.B., Liu, Z., Goble, R.J., Yi, S., 2009. Dune mobility and aridity at the desert margin of northern China at a time of peak monsoon strength. Geology 37 (10), 947–950.
Mischke, S., Zhang, C.J., Börner, A., Herzschuh, U., 2010. Lateglacial and Holocene variation in aeolian sediment flux over the northeastern Tibetan Plateau recorded by laminated sediments of a saline meromictic lake. Journal of Quaternary Science 25, 162–177.
Morrill, C., 2004. The influence of Asian summer monsoon variability on the water balance of a Tibetan lake. Journal of Paleolimnology 32, 273–286.
Morrill, C., Overpeck, J.T., Cole, J.E., 2003. A synthesis of abrupt changes in the Asian summer monsoon since the last deglaciation. The Holocene 13, 465–476.
Morrill, C., Overpeck, J.T., Cole, J.E., Liu, K.B., Shen, C.M., Tang, L.Y., 2006. Holocene variations in the Asian monsoon inferred from geochemistry of lake sediments in central Tibet. Quaternary Research 65, 232–243.
Murray, A.S., Wintle, A.G., 2000. Luminescence dating of quarts using an improved single-aliquot regenerative-dose procedure. Radiation Measurement 32, 57–73.
Overpeck, J.T., Anderson, D.M., Trumbore, S., Prell, W.L., 1996. The southwest Indian Monsoon over the last 18,000 years. Climate Dynamics 12, 213–225.
Partridge, T.C., 1993. Warming phases in the Southern Africa during the last 150,000 years—an overview. Palaleogeography, Palaeoclimatology, Palaeoecology 101, 237–244.
Porter, S.C., An, Z.S., 1995. Correlation between climate events in the North Atlantic and China during the last glaciation. Nature 375, 305–308.
Prescott, J.R., Hutton, J.T., 1994. Cosmic ray contributions to dose rates for luminescence and ESR dating: large depths and long term variations. Radiation Measurements 23, 497–500.
Qiang, M.R., Chen, F.H., Wang, Z.T., Niu, G.M., Song, L., 2010. Aeolian deposits at the southeastern margin of the Tengger Desert (China): Implications for surface wind strength in the Asian dust source area over the past 20,000 years. Palaeogeoraphy, Palaeoclimatology, Palaeoecology 286, 66–80.
Qiang, M.R., Song, L., Chen, F.H., Li, M.Z., Liu, X.X., Wang, Q., in press. A 16-ka lake-level record inferred from macrofossils in a sediment core from Genggahai Lake, northeastern Qinghai-Tibetan Plateau (China). Journal of Paleolimnology, doi: 10.1007/s10933-012-9660-z.
Rhode, D., Zhang, H.Y., Madsen, D.B., Gao, X., Brantingham, P.J., Ma, H.Z., Olsen, J.W., 2007. Epipaleolithic/early Neolithic settlements at Qinghai Lake, western China. Journal of Archaeological Science 34, 600–612.
Schlütz, F., Lehmkuhl, F., 2009. Holocene climatic change and the nomadic Anthropocene in Eastern Tibet: palynological and geomorphological results from the Nianbaoyeze Mountains. Quaternary Science Reviews 28, 1449–1471.
Shen, J., Liu, X.Q., Wang, S.M., Matsumoto, R., 2005. Palaeoclimatic changes in the Qinghai Lake area during the last 18,000 years. Quaternary International 136, 131–140.
Singhvi, A.K., Bluszcz, A., Bateman, M.D., Rao, M.S., 2001. Luminescence dating of loess-palaeosol sequences and coversands: methodological aspects and palaeoclimatic implications. Earth-Science Reviews 54, 193–211.
Stauch, G., IJmaker, J., Pötsch, S., Zhao, H., Hilgers, A., Diekmann, B., Dietze, E., Hartmann, K., Opitz, S., Wünnemann, B., Lehmkuhl, F., 2012. Aeolian sediments on the northeastern Tibetan Plateau. Quaternary Science Reviews 57, 71–84.
Stevens, T., Thomas, D.S.G., Armitage, S.J., Lund, H.R., Lu, H.Y., 2007. Reinterpreting climate proxy records from late Quaternary Chinese Loess: A detailed OSL investigation. Earth-Science Reviews 80, 111–136.
Stuiver, M., Groots, P.M., Braziunas, T.F., 1995. The GISP2 $\delta^{18}O$ climate record of the past 16,500 years and the roles of the sun, ocean and volcanoes. Quaternary Research 44, 341–354.
Sun, J.G., Li, B.G., Lu, Q., 2004. Temporal-spatial analysis of temperature and its effect on climate and water in Qinghai Gonghe Basin. Progress in Geography 23, 100–106 (in Chinese with English abstract).
Sun, J.M., Li, S.-H., Han, P., Chen, Y.Y., 2006. Holocene environmental changes in the central Inner Mongolian, based on single-aliquot-quartz optical dating and multi-proxy study of dune sands. Palaeogeoraphy, Palaeoclimatology, Palaeoecology 233, 51–62.
Sun, Y.J., Lai, Z.P., Long, H., Liu, X.J., Fan, Q.S., 2010. Quartz OSL dating of archaeological sites in Xiao Qaidam Lake of the NE Qinghai-Tibetan Plateau and its implications for palaeoenvironmental changes. Quaternary Geochronology 5, 360–364.
Sun, Y.J., Lai, Z.P., Madsen, D., Hou, G.L., 2012. Luminescence dating of a hearth from the archaeological site of Jiangxigou in the Qinghai Lake area of the northeastern Qinghai-Tibetan Plateau. Quaternary Geochronology 12, 107–110.
Telfer, M.W., Thomas, D.S.G., 2007. Late Quaternary linear dune accumulation and chronostratigraphy of the southwestern Kalahari: implications for aeolian palaeoclimatic reconstructions and predictions of future dynamics. Quaternary Science Reviews 26, 2617–2630.
Wang, Y.J., Cheng, H., Edwards, L.R., An, Z.S., Wu, J.Y., Shen, C.-C., Dorale, J.A., 2001. A high-resolution absolute-dated late Pleistocene monsoon record from Hulu Cave, China. Science 294, 2345–2348.
Wang, Y.J., Cheng, H., Edwards, R.L., He, Y.Q., Kong, X.G., An, Z.S., Wu, J.Y., Kelly, M.J., Dykoski, C.A., Li, X.D., 2005. The Holocene Asian Monsoon: links to solar changes and North Atlantic Climate. Science 308, 854–857.
Wang, Y.B., Liu, X.Q., Herzschuh, U., 2010. Asynchronous evolution of the Indian and East Asian Summer monsoon indicated by Holocene moisture patterns in monsoonal central Asia. Earth-Science Reviews 103, 135–153.
Wang, L., Li, J.J., Lu, H.Y., Gu, Z.Y., Rioual, P., Hao, Q.Z., Mackay, A.W., Jiang, W.Y., Cai, B.G., Xu, B., Han, J.T., Chu, G.Q., 2012. The East Asian winter monsoon over the last 15,000 years: its links to high-latitudes and tropical climate systems and complex correlation to the summer monsoon. Quaternary Science Reviews 32, 131–142.
Wintle, A.G., Murray, A.S., 2006. A review of Quartz optically stimulated luminescence characteristics and their relevance in single aliquot regeneration protocols. Radiation Measurements 41, 369–391.
Wischnewski, J., Mischke, S., Wang, Y.B., Herzschuh, U., 2011. Reconstructing climate variability on the northeastern Tibetan Plateau since the last Lateglacial—a multi-proxy, dual-site approach comparing terrestrial and aquatic signals. Quaternary Science Review 30, 82–97.
Xiao, J.L., Nakamura, T., Lu, H.Y., Zhang, G.Y., 2002. Holocene climate changes over the desert/loess transition of north-central China. Earth and Planetary Science Letter 197, 11–18.
Xu, S.Y., Xu, D.F., Shi, S.R., 1982. Aeolian sand deposits in the Gonghe Basin, Qinghai province. Journal of Desert Research 2, 1–8 (in Chinese with English abstract).
Xu, S.Y., Xu, D.F., Shi, S.R., 1984. A discussion on the development of landforms and evolution of environments in the Gonghe Basin. Journal of Lanzhou University 20, 146–157 (in Chinese with English abstract).
Yang, L.H., Wang, T., Zhou, J., Lai, Z.P., Long, H., 2012a. OSL chronology and possible forcing mechanisms of dune evolution in the Horqin dunefield in northern China since the Last Glacial Maximum. Quaternary Research 78, 185–196.
Yang, X.P., Li, H.W., Conacher, A., 2012b. Large-scale controls on the development of sand seas in northern China. Quaternary International 250, 74–83.
Yu, L.P., Lai, Z.P., 2012. OSL chronology and palaeoclimatic implications of aeolian sediments in the eastern Qaidam Basin of northeastern Qinghai-Tibetan Plateau. Palaeogeoraphy, Palaeoclimatology, Palaeoecology 337–338, 120–129.
Yu, X.F., Zhou, W.J., Liu, Z., Kang, Z.H., 2011. Different patterns of changes in the Asian summer and winter monsoons on the eastern Tibetan Plateau during the Holocene. The Holocene 21, 1031–1036.
Zeng, Y.N., Ma, H.Z., Sha, Z.J., Li, L.Q., Li, Z., Cao, G.C., 1999. The record of Younger Drays event in eolian sand deposits in Qaidam Basin. Chinese Geographical Science 9, 92–95 (in Chinese with English abstract).
Zeng, Y.N., Feng, Z.D., Cao, G.C., 2003. Desert formation and evolution in Qaidam Basin since the Last Glacial epoch. Acta Geographica Sinica 58, 452–457 (in Chinese with English abstract).
Zhang, J.W., Chen, F.H., Holmes, J.A., Li, H., Guo, X.Y., Wang, J.L., Li, S., Lü, Y.B., Zhao, Y., Qiang, M.R., 2011. Holocene monsoon climate documented by oxygen and carbon isotopes from lake sediments and peat bogs in China: a review and synthesis. Quaternary Science Reviews 30, 1973–1987.
Zhao, Y., Yu, Z.C., 2012. Vegetation response to Holocene climate change in East Asian monsoon-margin region. Earth-Science Reviews 113, 1–10.
Zhao, Y., Yu, Z.C., Chen, F.H., Zhang, J.W., Yang, B., 2009. Vegetation response to Holocene climate change in monsoon-influenced region of China. Earth-Science Reviews 97, 242–256.
Zhao, C., Yu, Z., Zhao, Y., Ito, E., Kodama, K.P., Chen, F., 2010a. Holocene millennial-scale climate variations documented by multiple lake-level proxies in sediment cores from Hurleg Lake, Northwest China. Journal of Paleolimnology 44, 995–1008.
Zhao, H., Lu, Y.C., Wang, C.M., Chen, J., Liu, J.F., Mao, H.L., 2010b. ReOSL dating of aeolian and fluvial sediments from Nihewan Basin, northern China and its environmental application. Quaternary Geochronology 5, 159–163.
Zhu, Z.D., 1980. An Outline on Chinese Deserts. Science Press, Beijing (in Chinese).